A Kernel-based Approach to Diffusion Tensor and Fiber Clustering in the Human Skeletal Muscle

Radhouène Neji, Jean-François Deux, Gilles Fleury, Mezri Maatouk, Georg Langs, Jean-Philippe Thiran, Guillaume Bassez, Alain Rahmouni, Nikolaos Paragios

INRIA

INSTITUT NATIONAL DE RECHERCHE EN INFORMATIQUE ET EN AUTOMATIQUE

A Kernel-based Approach to Diffusion Tensor and Fiber Clustering in the Human Skeletal Muscle

Radhouène Neji — Jean-François Deux — Gilles Fleury — Mezri Maatouk — Georg Langs — Jean-Philippe Thiran — Guillaume Bassez — Alain Rahmouni — Nikos Paragios

N° 6686

October 2008

Thème BIO

Rapport de recherche

ISSN 0249-6399 ISRN INRIA/RR--6686--FR+ENG

A Kernel-based Approach to Diffusion Tensor and Fiber Clustering in the Human Skeletal Muscle

Radhouène Neji* , Jean-François Deux , Gilles Fleury , Mezri Maatouk , Georg Langs , Jean-Philippe Thiran , Guillaume Bassez , Alain Rahmouni , Nikos Paragios

Thème BIO — Systèmes biologiques
Projet Galen

Rapport de recherche n° 6686 — October 2008 — 23 pages

Abstract: In this report, we present a kernel-based approach to the clustering of diffusion tensors in images of the human skeletal muscle. Based on the physical intuition of tensors as a means to represent the uncertainty of the position of water protons in the tissues, we propose a Mercer (i.e. positive definite) kernel over the tensor space where both spatial and diffusion information are taken into account. This kernel highlights implicitly the connectivity along fiber tracts. We show that using this kernel in a kernel-PCA setting compounded with a landmark-Isomap embedding and k-means clustering provides a tractable framework for tensor clustering. We extend this kernel to deal with fiber tracts as input using the multi-instance kernel by considering the fiber as set of tensors centered in the sampled points of the tract. The obtained kernel reflects not only interactions between points along fiber tracts, but also the interactions between diffusion tensors. We give an interpretation of the obtained kernel as a comparison of soft fiber representations and show that it amounts to a generalization of the Gaussian kernel Correlation. As in the tensor case, we use the kernel-PCA setting and k-means for grouping of fiber tracts. This unsupervised method is further extended by way of an atlas-based registration of diffusion-free images, followed by a classification of fibers based on non-linear kernel Support Vector Machines (SVMs) and kernel diffusion. The experimental results on a dataset of diffusion tensor images of the calf muscle of 25 patients (of which 5 affected by myopathies, i.e. neuromuscular diseases) show the potential of our method in segmenting the calf in anatomically relevant regions both at the tensor and fiber level.

Key-words: DTI, Diffusion tensor, Fiber, Kernels, Clustering, Human skeletal muscle

* This work was carried out while the author was at the Signal Processing Laboratory of the Swiss Federal Institute of Technology, Lausanne (EPFL).

Unité de recherche INRIA Futurs
Parc Club Orsay Université, ZAC des Vignes,
4, rue Jacques Monod, 91893 ORSAY Cedex (France)
Téléphone : +33 1 72 92 59 00 — Télécopie : +33 1 60 19 66 08

Une approche basée sur des noyaux pour le groupement de tenseurs de diffusion et de fibres dans le muscle squelettique

Résumé : Dans ce rapport, nous présentons une approche basée sur des noyaux pour le groupement de fibres dans le muscle squelettique. En se basant sur l'intuition physique derrière les tenseurs de diffusion comme moyen de représenter l'incertitude sur la position des molécules d'eau dans les tissus, nous proposons un noyau de Mercer (défini positif) sur l'espace des tenseurs qui tient compte aussi bien de l'information spatiale que de l'information de diffusion. Le noyau met l'accent implicitement sur la connectivité le long des fibres. Nous montrons que l'utilisation de ce noyau pour une analyse en composantes principales combinée à l'algorithme Isomap fournit un cadre pratique pour regrouper les tenseurs. Nous étendons ce noyau pour pouvoir segmenter des fibres en considérant une fibre comme étant un ensemble de tenseurs centrés sur les points échantillonés le long de sa trajectoire. Le noyau obtenu reflète aussi bien les intéractions spatiales que les intéractions entre tenseurs de diffusion. Nous donnons également une interprétation de ce noyau comme étant une faqn de comparer des représentations probabilistes des fibres. Nous étendons la méthode pour effectuer une segmentation supervisée à l'aide d'un atlas en utilisant des SVMs non linéaires combinés avec une diffusion base sur un champ de Markov. Les résultats expérimentaux effectués sur les données de mollet de 25 patients (dont 5 atteints de myopathies) montrent le potentiel de notre méthode pour segmenter le muscle en régions anatomiquement significatives.

Mots-clés : IRM de diffusion, Tenseur de diffusion, Fibre, Noyaux, Groupement, Muscle squelettique

Contents

1 Introduction

1.1 Context and Motivation

Diffusion Tensor Imaging (DTI) is a modality that has been used extensively in the study of the connectivity within the different anatomical structures in the human brain [1]. The acquisition setting allows to compute a field of 3×3 symmetric positive definite matrices that model the uncertainty information (covariance) of a Gaussian distribution over the displacements of water protons in the tissues. DTI has attracted much interest because of its potential in unveiling the fiber tracts in brain white matter, since diffusive transport in organized tissues is more important along fiber directions and is rather hindered in the orthogonal directions. However, little work has been done to harness the potential of this modality to explore other regions where water diffusion can carry rich information about the architecture of the fibers and the underlying structure and organization. The human skeletal muscles and more specifically the lower leg are of particular interest because they present an ordered structure of elongated myofibers. Moreover, the perspective of studying the effect of neuromuscular diseases (myopathies) on water diffusion in the human skeletal muscle and providing a tool for early diagnosis and quantitative assessment of muscular weakness and atrophy due to illness based on DTI information is enticing. For the time being, it is unclear how the muscular diseases affect the myofibers, therefore separating the different muscle groups of the skeletal muscles of the lower leg (calf) in regions consistent with anatomical knowledge is a crucial step for a localized quantitative study and comparison of healthy and diseased fiber bundles.

In the following, we review the existing methods for tensor and fiber clustering.

1.2 Previous Work

1.2.1 Diffusion Tensor Clustering

The existing diffusion tensor clustering algorithms can be subdivided in three groups. The first class of methods uses a variational approach along with an adequate distance over the manifold of 3×3 symmetric positive definite matrices. For instance in [2], a 3D surface is evolved using an implicit level set representation to segment a region of interest where the spatial gradient is computed using the geodesic distance and the distributions of the tensors in each region are modeled as Gaussian. In [3], the Mumford-Shah functional is minimized using a distance between tensors derived from the Burg divergence. A level set technique is also used in [4] to extract the cingulum based on the Finsler metric. Similarly in [5], several similarity measures are investigated and guide the evolution of coupled level sets.

The second class of methods uses common clustering algorithms to achieve segmentation of the tensor field. In [6], the authors propose to use the Log-Euclidean metric to obtain a kernel density estimate of the probability distribution of tensors and include it in a fuzzy k-means framework where the spatial interactions are handled using local Gaussian kernels

with a fixed bandwidth. In [7], mean-shift clustering is applied for the segmentation of the Thalamus using Gaussian kernels both in the tensor and in the position space.

The third class of methods consists of graph theoretical approaches and manifold learning techniques that try to capture the structure of the tensor field and propagate the information between neighbors. In [8], a graph-cut approach is used with seed-point initialization. Spectral clustering is performed in [9] through the eigenanalysis of an affinity matrix between tensors based on a selected similarity measure. In [10], several manifold learning techniques are extended to deal with non-Euclidean spaces and spatial connectivity is ensured by considering isotropic neighborhoods. The particular case of Locally Linear Embedding (LLE) is further discussed in [11] with different choices of tensor metrics.

1.2.2 Fiber Clustering

Graph theoretical approaches have been particularly popular for fiber clustering. For instance, a Gaussian model of the fibers and a normalized-cut approach based on the Euclidean distance between the moments is presented in [12]. In [13], spectral clustering along with the Hausdorff distance between fibers is considered. The method presented in [14] relies on Laplacian Eigenmaps and similarity between fibers is determined using their end points. In [15], the authors suggest another manifold learning technique by constructing a graph-based distance that captures local and global dissimilarities between fibers and use LLE for clustering of the tracts. Curve modeling has attracted attention and was handled in [16] by defining a spatial similarity measure between curves and using the Expectation-Maximization algorithm for clustering. More recently, fibers were represented in [17] using their differential geometry and frame transportation and a consistency measure was used for clustering

Of particular interest in the field are the supervised methods that try to achieve a segmentation consistent with a predefined atlas. Registration of B0 images and a hierarchical classification of fibers is performed in [18] using the B-spline representation of fibers. The method proposed in [13] is further extended in [19] by means of a Nystrom approximation of the out-of-sample extension of the spectral embedding.

1.3 Contributions of this Work

We address several issues in this report. While the previous fiber clustering methods discard the tensor information and rely on the obtained tracts, the method we propose handles tensors and is easily extended to segment fibers while taking into account the initial tensor field. We also bridge the gap between tensor and fiber clustering. To this end, we propose a kernel over the tensor space that is consistent with the physical intuition of diffusion tensors as representing the covariance of the probability distribution of water protons positions. Unlike the existing similarity measures and the use of isotropic Gaussian kernels or neighborhoods for spatial interaction, the proposed kernel quantifies not only the dissimilarity between tensors, but takes into account their localization in space in a tractable way and enhances implicitly the connectivity along fiber tracts, i.e. in the feature space provided by the kernel embedding, tensors which are aligned will be closer than tensors which do not lie

on the same fiber tract, which is not guaranteed by spatially isotropic Gaussian kernels. We use kernel-PCA for embedding in a Euclidean space and landmark-Isomap for information propagation along diffusive pathways to obtain the final embedding. This is important as it allows to reflect the diffusion flow along the muscle fibers which are characterized by an elongated structure. The clustering is done in the embedding space by a plain k-means algorithm.

The proposed kernel is extended to deal with fiber tracts as input of the clustering algorithm by way of the summation kernel, which is a handy way to define kernels over sets. Not only we take into account in this kernel the interactions between the points (as spatial positions) but also the information provided by the whole tensor field. Given that the fiber pathways are provided, only kernel-PCA and k-means are sufficient for clustering in the fiber domain. We give an interpretation of the fiber kernel as a comparison of soft representations of the fiber tracts and show that it provides a natural generalization for Gaussian kernel Correlation.

In a last step, we show how this unsupervised algorithm can be made supervised in an efficient way. Unlike the work in [19], given that the kernel satisfies the Mercer conditions, we can look at the problem from a discriminative perspective and avoid the Nystrom out-of-sample extension by using a kernel SVM classification and Markov Random Field kernel diffusion of the obtained classification scores in order to segment the calf muscle in regions consistent with a previously defined atlas.

The remainder of this report is organized as follows: In section 2, we discuss the kernel over the tensor space and provide an analysis of its properties and advantages. We also discuss its use in a kernel-PCA and landmark-Isomap setting for clustering of diffusion tensors. Based on the summation kernel, we provide an extension of this kernel to deal with fiber tracts in section 3, where we also discuss the interpretation of the obtained kernel as a means to measure similarity between soft representations of the fiber tracts. We discuss also the special case of Gaussian kernel Correlation. In section 4, we provide the supervised version of the algorithm based on kernel SVMs and kernel diffusion. Section 5 is dedicated to the experimental results and we discuss the perspectives of this work in section 6.

2 A Probability Kernel on Tensors

Diffusion tensors measure the motion distribution of water molecules. More explicitly, they refer to the covariance of a Gaussian probability over the displacements $\mathbf{r}$ of the water protons given a diffusion (mixing) time t:

$$p(\mathbf{r}|t,\mathbf{D}) = \frac{1}{\sqrt{\det(\mathbf{D})(4\pi t)^3}} \exp\left(-\frac{\mathbf{r}^t\mathbf{D}^{-1}\mathbf{r}}{4t}\right) \quad (1)$$

Given a diffusion tensor $\mathbf{D}$ localized at voxel $\mathbf{x}$, we can obtain the probability of the position y of the water molecule previously localized at $\mathbf{x}$ in a straightforward way:

$$p(\mathbf{y}|\mathbf{x},t,\mathbf{D}) = \frac{1}{\sqrt{\det(\mathbf{D})(4\pi t)^3}} \exp\left(-\frac{(\mathbf{y}-\mathbf{x})^t\mathbf{D}^{-1}(\mathbf{y}-\mathbf{x})}{4t}\right) \tag{2}$$

Therefore, a natural way to define a kernel over the tensor space where position is taken into account is to consider the expected likelihood kernel [20]. Let us consider two tensors $\mathbf{D}_1$ and $\mathbf{D}_2$ localized at $\mathbf{x}_1$ and $\mathbf{x}_2$ respectively, and a diffusion time t. The expected likelihood kernel $k_t((\mathbf{D_1},\mathbf{x}_1);(\mathbf{D_2},\mathbf{x}_2))$ between the pairs $(\mathbf{D_1},\mathbf{x}_1)$ and $(\mathbf{D_2},\mathbf{x}_2)$ is defined as the expectation of Gaussian probability $p_2(\mathbf{y}|\mathbf{x_1},t,\mathbf{D}_1)$ under the probability law of $p_1(\mathbf{y}|\mathbf{x_2},t,\mathbf{D}_2)$ and is given by the following expression:

$$\begin{aligned} k_t((\mathbf{D_1},\mathbf{x}_1);(\mathbf{D_2},\mathbf{x}_2)) &= E_{p_2(\mathbf{y}|\mathbf{x_2},t,\mathbf{D}_2)}(p_1(\mathbf{y}|\mathbf{x_1},t,\mathbf{D}_1)) &(3)\\ &= \int p_1(\mathbf{y}|\mathbf{x_1},t,\mathbf{D}_1)p_2(\mathbf{y}|\mathbf{x_2},t,\mathbf{D}_2)d\mathbf{y} &(4)\end{aligned}$$

Note that the diffusion time t is naturally a parameter for this kernel. Using the expression provided in 2, one can obtain the following closed-form expression of this kernel:

$$k_t((\mathbf{D_1},\mathbf{x}_1);(\mathbf{D_2},\mathbf{x}_2)) = \frac{1}{\sqrt{(4\pi t)^3}} k_1(\mathbf{D_1},\mathbf{D_2})k_2((\mathbf{D_1},\mathbf{x}_1);(\mathbf{D_2},\mathbf{x}_2)) \tag{5}$$

where

$$\begin{aligned} k_1(\mathbf{D_1},\mathbf{D_2}) &= \frac{1}{\sqrt{\det(\mathbf{D}_1+\mathbf{D}_2)}}\\ k_2((\mathbf{D_1},\mathbf{x}_1);(\mathbf{D_2},\mathbf{x}_2)) &= \exp\left(-\frac{1}{4t}(\mathbf{x}_1^t\mathbf{D}_1^{-1}\mathbf{x}_1+\mathbf{x}_2^t\mathbf{D}_2^{-1}\mathbf{x}_2)\right) \times\\ &\quad \exp\left(\frac{1}{4t}(\mathbf{D}_1^{-1}\mathbf{x}_1+\mathbf{D}_2^{-1}\mathbf{x}_2)^t(\mathbf{D}_1^{-1}+\mathbf{D}_2^{-1})^{-1}(\mathbf{D}_1^{-1}\mathbf{x}_1+\mathbf{D}_2^{-1}\mathbf{x}_2)\right) \end{aligned} \tag{6}$$

2.1 Properties of the Tensor Kernel

The kernel stems from an L^2 inner product defined on the Hilbert space of square-integrable functions, to which Gaussian probability densities belong. Therefore the kernel verifies the Mercer conditions, i.e. it is positive definite. We hereafter provide an analysis of this kernel:

- The first term $k_1(\mathbf{D_1},\mathbf{D_2})$ may be rewritten as follows:

$$k_1(\mathbf{D_1},\mathbf{D_2}) = \frac{1}{\sqrt{\det(\mathbf{D}_2)}}\frac{1}{\sqrt{\det(\mathbf{Id}+\mathbf{D}_1\mathbf{D}_2^{-1})}} = \frac{1}{\sqrt{\det(\mathbf{D}_1)}}\frac{1}{\sqrt{\prod_{i=1}^3(1+\lambda_i)}} \tag{7}$$

where $\mathbf{Id}$ is the 3×3 identity matrix and λ_i are the generalized eigenvalues of the pair of matrices $(\mathbf{D}_1, \mathbf{D}_2)$. This is reminiscent of the geodesic distance on the manifold of 3×3 symmetric positive definite matrices $d = \sqrt{\sum_{i=1}^{3}(\log(\lambda_i))^2}$ [21] which is also based on the generalized eigenvalues: the distance (respectively the kernel) is increasing (respectively decreasing) with increasing (respectively decreasing) generalized eigenvalues, which is a reasonable behavior (recall that the kernel reflects similarity). The symmetry is ensured in the geodesic distance by the squared logarithm function because the latter is invariant with respect to the inverse transformation $\lambda_i \mapsto \frac{1}{\lambda_i}$ (recall that the generalized eigenvalues of the pair $(\mathbf{D}_2, \mathbf{D}_1)$ are the inverse of those of the pair $(\mathbf{D}_1, \mathbf{D}_2)$), while it can be seen that the factor $\frac{1}{\sqrt{\det(\mathbf{D}_2)}}$ has a similar role since it also preserves the symmetry. Note that the original expression is clearly symmetric.

- Two special cases of the second factor k_2 are interesting:
  1. When $\mathbf{D}_1 = \mathbf{D}_2 = \mathbf{D}$
  $$k_2((\mathbf{D}, \mathbf{x}_1); (\mathbf{D}, \mathbf{x}_2)) = \exp\left(-\frac{1}{8t}(\mathbf{x}_1 - \mathbf{x}_2)^t \mathbf{D}^{-1}(\mathbf{x}_1 - \mathbf{x}_2)\right) \tag{8}$$
  As expected, when the tensors are equal, what appears is the Mahalanobis distance between positions $\mathbf{x}_1$ and $\mathbf{x}_2$ with respect to $\mathbf{D}$. In particular when the tensor $\mathbf{D}$ is isotropic, i.e. $\mathbf{D} = \mu\mathbf{Id}$, $k_2((\mathbf{D}, \mathbf{x}_1); (\mathbf{D}, \mathbf{x}_2)) = \exp\left(-\frac{1}{8\mu t}||\mathbf{x}_1 - \mathbf{x}_2)||^2\right)$, which is plainly a Gaussian kernel between the points $\mathbf{x}_1$ and $\mathbf{x}_2$.
  2. When $\mathbf{x}_1 = \mathbf{x}_2 = \mathbf{x}$, $k_2((\mathbf{D}_1, \mathbf{x}); (\mathbf{D}_2, \mathbf{x})) = 1$, which means that the kernel k reduces to k_1. Again this was expected since the kernel will rely only on tensor similarity if there is no difference in spatial positions.
- The first special case is of particular interest in diffusion tensor analysis to enhance the connectivity between tensors which are aligned on the same fiber tract. Let us consider the tensor configuration in figure 1 where all tensors are equal to $D = \mu(\vec{\mathbf{e}_1}\vec{\mathbf{e}_1}^t + \vec{\mathbf{e}_2}\vec{\mathbf{e}_2}^t) + \nu\, \vec{\mathbf{e}_3}\vec{\mathbf{e}_3}^t$, where $(\vec{\mathbf{e}_i})_{i=1\ldots3}$ are the canonical basis of $\mathbb{R}^3$ and $\nu > \mu$ are the eigenvalues of D. The tensors have therefore a principal direction of diffusion along $\vec{\mathbf{e}_3}$. The tensors are all equal yet the second term k_2 allows to affect more affinity between tensors 1 and 2 than between tensors 1 and 3. Indeed, we can compute the kernel values to obtain
  $$k_2((\mathbf{D}, \mathbf{x}_1); (\mathbf{D}, \mathbf{x}_2)) = \exp\left(-\frac{d^2}{8\nu t}\right) \tag{9}$$
  $$k_2((\mathbf{D}, \mathbf{x}_1); (\mathbf{D}, \mathbf{x}_3)) = \exp\left(-\frac{d^2}{8\mu t}\right) \tag{10}$$
  where $d = ||\mathbf{x}_1 - \mathbf{x}_2|| = ||\mathbf{x}_1 - \mathbf{x}_3||$. Since $\nu > \mu$, we can see that the similarity between the tensors 1 and 2 is higher than the similarity the tensors 1 and 3, despite the fact that the tensors are all equal.The kernel captures locally the fiber structure.

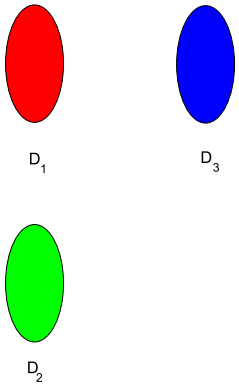

Figure 1: A configuration where the tensor kernel implicitly puts more weight on the connection between $\mathbf{D}_1$ and $\mathbf{D}_2$ than between $\mathbf{D}_1$ and $\mathbf{D}_3$, reflecting their alignment.

2.2 Embedding of the Tensors through Kernel PCA and Landmark Isomap

Let us consider the N pairs $(\mathbf{D}_i, \mathbf{x}_i)_{i=1...N}$ representing a tensor field. We construct the $N \times N$ kernel matrix $\mathbf{K}$ of entries $\mathbf{K}_{ij} = k_t((\mathbf{D}_i, \mathbf{x}_i); (\mathbf{D}_j, \mathbf{x}_j))$ for a fixed diffusion time t and normalize it to obtain $\widetilde{\mathbf{K}}$ such that $\widetilde{\mathbf{K}}_{ij} = \frac{\mathbf{K}_{ij}}{\sqrt{\mathbf{K}_{ii}\mathbf{K}_{jj}}}$. These pairs are then embedded in a k-dimensional Euclidean space using an eigenvalue decomposition of $\widetilde{\mathbf{K}} = \mathbf{U}\mathbf{S}\mathbf{U}^t$ where $\mathbf{U}$ is an orthogonal $N \times k$ matrix and $\mathbf{S}$ is a $k \times k$ diagonal matrix. The coordinates of the embedded tensors are given by the $N \times k$ matrix $\mathbf{X} = \mathbf{U}\sqrt{\mathbf{S}}$ where $\sqrt{\mathbf{S}}$ is obtained by setting the diagonal elements of $\mathbf{S}$ to their square roots [22]. Each row m of $\mathbf{X}$ holds the coordinates in the feature space of the m-th pair.

Given the k-dimensional representation $\mathbf{X}$ of the tensor field, one has to propagate the local interaction between the tensors and take into account the distance along diffusive pathways, i.e. simulate the water flow along these trajectories. This is done using the Isomap algorithm which is based on two steps [23]:

1. Between every two points of the dataset, find the shortest path using the Dijkstra algorithm based on the Euclidean distance in the feature space and compute a new distance matrix that holds the lengths of the path. This step is important in diffusion tensor analysis in order to propagate diffusion information along fiber tracts.

2. Perform Multidimensional Scaling (MDS) to obtain the new embedding, i.e. a configuration of points that respects approximately the distance matrix computed in the previous step. Since the kernel enhances fiber connectivity, we expect the new configuration to reflect the diffusion flow in the tissues.

Note that in practice we use a faster version of this algorithm called landmark-Isomap [24] that reduces the computational time of the first step by computing the distance of the points to a reduced set of landmarks chosen randomly in the dataset. The clustering is done afterwards using a plain k-means algorithm. Note that the kernel PCA step amounts to denoising in the feature space and that from a theoretical point of view (with perfect data), we could have used from the outset the Euclidean distance (L^2 norm) implied by the kernel k_t in the Isomap algorithm without the kernel PCA projection, since the latter requires only the distances between points given by the following expression:

$$d = \sqrt{k_t((\mathbf{D_1}, \mathbf{x}_1); (\mathbf{D_1}, \mathbf{x}_1)) + k_t((\mathbf{D_2}, \mathbf{x}_2); (\mathbf{D_2}, \mathbf{x}_2)) - 2k_t((\mathbf{D_1}, \mathbf{x}_1); (\mathbf{D_2}, \mathbf{x}_2))} \quad (11)$$

In the following section, we extend in a tractable way the proposed kernel defined over the tensor field to the fiber domain.

3 Probability Kernel in the Fiber Domain

The fiber trajectories are obtained through the integration of the vector field of principal directions of diffusion. Based on the continuous tensor field approximation (by means of interpolation), we represent each fiber tract as a sequence of tensors localized in spatial positions, i.e. is a set of pairs $\tau_i = (\mathbf{D}_i, \mathbf{x}_i)_{i=1...n}$ where n is the number of points lying on the fiber. Note that the tractography already requires tensor interpolation and that the interpolated tensors are therefore kept for kernel computation. So it is natural to extend the tensor kernel using a kernel over sets. We simply use the summation kernel [25] to obtain the following Mercer kernel K_t between two fibers $\mathbf{F}_1$ and $\mathbf{F}_2$:

$$K_t(\mathbf{F}_1, \mathbf{F}_2) = \frac{1}{n_1}\frac{1}{n_2} \sum_{(\mathbf{D}_i, \mathbf{x}_i) \in \mathbf{F}_1} \sum_{(\mathbf{D}_j, \mathbf{x}_j) \in \mathbf{F}_2} k_t((\mathbf{D}_i, \mathbf{x}_i); (\mathbf{D}_j, \mathbf{x}_j)) \quad (12)$$

where n_1 (resp. n_2) is the number of points of the fiber $\mathbf{F}_1$ (resp. $\mathbf{F}_2$). This kernel sums the interactions between tensors belonging to the fiber tracts. It captures the diffusion and spatial links between diffusive pathways. It is important to notice that while all the interactions are summed, the diffusion time t acts as a scale parameter. Therefore for a suitable choice of t, a tensor interacts only with tensors lying in a local neighborhood and far-away tensors have a negligible impact on the summation. As in the case of tensors, the segmentation of the fiber tracts is achieved using kernel PCA and k-means clustering.

3.1 A Physical Interpretation of the Fiber Kernel

One can see that the summation kernel is simply the expected likelihood kernel between distributions providing a soft representation for fibers. More explicitly, we consider a dynamical system where a particle can be initially at a position $\mathbf{x}_i$ on the fiber tract and moves

to a position y with the following probability

$$p(y|t,(\mathbf{D}_i)_{i=1\ldots n}) = \sum_{i=1}^{n} p(\mathbf{x}_i)p(\mathbf{y}|\mathbf{x}_i,t,\mathbf{D}_i) \tag{13}$$

With a uniform prior distribution on $\mathbf{x}_i$, $p(y|t,(\mathbf{D}_i)_{i=1\ldots n}) = \frac{1}{n}\sum_{i=1}^{n} p(\mathbf{y}|\mathbf{x}_i,t,\mathbf{D}_i)$. If the initial positions were independent (which is not the case because they are the result of the tractography), this would have amounted exactly to an *adaptive* kernel density estimation of the position of the water molecules along the fiber tracts where the point-dependent Gaussian kernels use the diffusion tensors as covariance matrices to model the uncertainty. However the distributions in equation 13 still provide a soft representation of the fibers and measure the compactness of the spatial configuration of the fiber tract. By bilinearity of the expected likelihood kernel, it is straightforward to see that the expected likelihood kernel of the distributions given in Equation 13 is exactly the summation kernel.

3.2 Links with Gaussian Kernel Correlation

When considering the special case where the tensor field is constant (equal to a tensor $\mathbf{D}$), we obtain

$$K_t(\mathbf{F}_1,\mathbf{F}_2) \propto \frac{1}{n_1}\frac{1}{n_2}\sum_{\mathbf{x}_i\in\mathbf{F}_1}\sum_{\mathbf{x}_j\in\mathbf{F}_2}\exp\left(-\frac{1}{8t}(\mathbf{x}_i-\mathbf{x}_j)^t\mathbf{D}^{-1}(\mathbf{x}_i-\mathbf{x}_j)\right) \tag{14}$$

which is the anisotropic form of the Gaussian kernel correlation [26]:

$$KG_t(\mathbf{F}_1,\mathbf{F}_2) \propto \frac{1}{n_1}\frac{1}{n_2}\sum_{\mathbf{x}_i\in\mathbf{F}_1}\sum_{\mathbf{x}_j\in\mathbf{F}_2}\exp\left(-\frac{||\mathbf{x}_i-\mathbf{x}_j)||^2}{8\mu t}\right) \tag{15}$$

where $\mathbf{D} = \mu\mathbf{Id}$ which means that we suppose the tensors are isotropic. We can see that the proposed kernel deals with a generic tensor field and provides a generalization of the Gaussian kernel correlation. A by-product of this reasoning is that Gaussian kernel correlation is a kernel on fibers that considers only point positions. One could have seen from the outset that is a Mercer kernel since it is a summation of Mercer (Gaussian) kernels. This will be particularly useful to learn spatial interactions between fibers as it will be detailed in the next section.

4 A Supervised Fiber Clustering Framework

4.1 Supervised Kernel SVM Learning of Atlas Fibers

Given an atlas of fibers segmented by an expert in R regions, we can learn the spatial interactions between these fibers using the Gaussian kernel correlation in Equation 15. Indeed, it can be used as an input in a kernel Support Vector Machines (SVMs) [27] to learn

boundaries between the different segmented regions, including background fibers that are not localized in the region of interest. The kernel SVMs provide support vectors (fibers), which are the fibers that define the decision boundaries. Note that the SVMs are used in a one-against-one fashion in order to deal with multiple regions. A point of interest here is that from the initial set of training fibers, we have only to keep a sparse subset of support fibers that will guide the classification process. The fact that the Gaussian kernel correlation defines a kernel allows to avoid the Nystrom approximation of the out-of-sample extension of the spectral embedding proposed in [19] by looking to the problem from a discriminative perspective as opposed to a projection approach.

Given a new set of fibers that we wish to segment in a manner consistent with the already-defined atlas, we start by finding the affine transformation that maps the diffusion-free (B0) image of the training atlas to the corresponding one in the testing dataset, as in [18]. This tranformation is subsequently used to register the testing set of fibers to the space of the support fibers obtained from the atlas. We are therefore able to compute the scores of the $\frac{R(R-1)}{2}$ pairwise SVM classifiers on the testing dataset. In the following subsection, we show how to use the SVM classification results to obtain the segmentation while respecting the interactions provided by the fiber kernel.

4.2 Markov Random Field Segmentation of the Fiber Tracts

We start by embedding the fibers that are to be segmented in a k-dimensional space using kernel PCA. Then for each fiber, we consider its k-nearest neighbors according to the Euclidean distance in the feature space. Based on the defined spatial neighborhoods, we use a Markov random field model and minimize the following energy:

$$E = \sum_{\mathbf{F}_i} u^s(l(\mathbf{F}_i)) + \lambda \sum_{\mathbf{F}_i, \mathbf{F}_j \in \mathcal{N}(\mathbf{F}_i)} u^p(l(\mathbf{F}_i), l(\mathbf{F}_j)) \tag{16}$$

where $l(\mathbf{F_i})$ is the classification label of the fiber $\mathbf{F}_i$ and $\mathcal{N}(\mathbf{F}_i)$ its neighborhood.

The first term is provided by the classifiers (data term) and set to $u^s(l(\mathbf{F}_i)) = -\log(\frac{2k_l}{R(R-1)})$ where k_l is the number of pairwise classifiers voting for class l (if $k_l = 0$, we choose $u^s(l(\mathbf{F}_i)) = -\log(\epsilon)$, where ϵ is a relatively low value).

The second term is used for kernel-based regularization and set to $u^p(l(\mathbf{F}_i), l(\mathbf{F}_j)) = K_t(\mathbf{F}_i, \mathbf{F}_j)(1 - \delta(l(\mathbf{F}_i), l(\mathbf{F}_j)))$ where δ is the Kronecker delta. The constant λ is a trade-off parameter between the two terms. This amounts to a kernel graph diffusion of the initial labels provided by the SVM classifiers and accounts for the regularity of the segmentation. The energy is optimized using the algorithm described in [28].

5 Results and Experiments

The human skeletal muscles and more specifically the lower leg are of particular interest because they present an ordered structure of elongated myofibers where some muscle groups

differ only subtly in their direction. In order to study the effect of neuromuscular diseases (myopathies) on water diffusion in the muscles, segmentation in regions consistent with anatomical knowledge is a crucial preliminary step before a localized quantitative study of diffusion properties in the fiber bundles for healthy and diseased tissues. Diffusion-based studies of the human skeletal muscle [29, 30, 31] focused on studying variation across subjects of scalar information like diffusivity (trace), fractional anisotropy, pennation angles (the orientation of muscular fibers with respect to tendons), etc. A supervised SVM tensor classification algorithm was proposed in [32].

Twenty-five subjects (twenty healthy patients and five patients affected by myopathies) underwent a diffusion tensor imaging of the calf muscle using a 1.5 T MRI scanner. The following parameters were used : repetition time (TR)= 3600 ms, echo time(TE) = 70 ms, slice thickness = 7 mm and b value of 700 $s.mm^{-2}$ with 12 gradient directions and 13 repetitions. The size of the obtained volumes is $64 \times 64 \times 20$ voxels with a voxel resolution of $3.125\,mm \times 3.125\,mm \times 7\,mm$. We acquired simultaneously high resolution T1-weighted images that were segmented manually by an expert into 7 muscle groups to provide the ground truth and fiber trajectories were reconstructed using [33]. To give an idea about the muscle architecture in the calf, we present in [Fig.2 (a)] a manual segmentation overlaid on an axial slice of a high-resolution T1-weighted image. The following muscle groups are considered: the soleus (SOL), lateral gastrocnemius (LG), medial gastrocnemius (MG), posterior tibialis (PT), anterior tibialis (AT), extensor digitorum longus (EDL), and the peroneus longus (PL).

In the following , we present the obtained experimental results on a synthetic dataset and for tensor classification and both supervised and unsupervised fiber bundling of the lower leg muscles.

5.1 Tensor Clustering

5.1.1 Preliminary Experiments

We first generated a 20×40 lattice of synthetic tensors composed of two close fiber bundles. The first bundle has a vertical principal direction, the second starts with a vertical direction then deviates with a 45° angle [Fig.3 (a)]. We added a Gaussian noise of standard deviation 10° to these directions. The eigenvalues of the tensors were set to $\{2\,10^{-3}, 1.5\,10^{-3}, 10^{-3}\}$. We tested the following values of diffusion time t: $\{10^4, 10^5\}$. We compare the behavior of the kernel PCA + Isomap embedding with spectral clustering using the metric $d(\mathbf{D_1}, \mathbf{D_2}) = \arccos(<\vec{\mathbf{e}_1}, \vec{\mathbf{e}_2}>)$ where $\vec{\mathbf{e}_1}$ (resp. $\vec{\mathbf{e}_2}$) is the principal direction of diffusion of $\mathbf{D}_1$ (resp. $\mathbf{D}_2$), as in [9]. Following [9], the scale parameter in the affinity matrix is set as the sample variance of d between neighboring tensors. The clustering is obtained using k-means with 50 restarts in the spectral embedding space. [Fig.3 (c)] shows the segmentation result obtained by our approach (stable across the tested set of diffusion times) and [Fig.3 (b)] shows its counterparts for spectral clustering. We can notice that unlike spectral clustering, the proposed algorithm finds a clustering solution which is more compatible with the tensor

(a) (b)

Figure 2: (a) An example of a manual segmentation of an axial slice of a high-resolution T1-weighted image showing different muscle groups in the calf. (b) An axial slice of a T1-weighted image of the calf of a diseased patient where the zone in hypertension is fat that replaced the muscle.

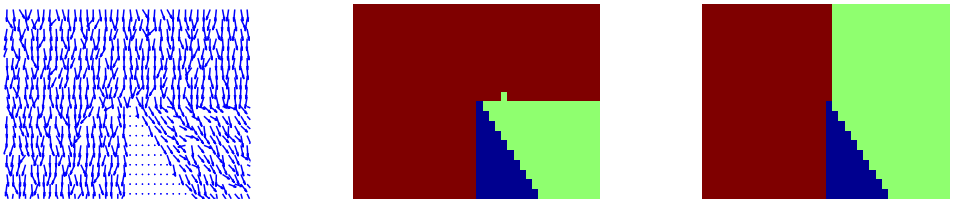

(a) (b) (c)

Figure 3: (a) Synthetic noisy field of principal directions of diffusion. (b) Result of spectral clustering. (c) Result of our method

arrangement. This is due to the fact that it captures both tensor similarity and spatial connectivity.

To further assess qualitatively the method, we used the proposed kernel PCA + Isomap embedding to see if it is faithful to the known structure of the muscles. Of particular interest is the soleus which is a major part of the calf. It has a bipennate structure where oblique fibers converge towards a central aponeurosis [Fig.4 (c)]. In [Fig.4 (a), (b)], we show the (here three-dimensional) proposed embedding for the soleus muscle of one subject for $t = 2\ 10^5$. The obtained points reveal the structure of the muscle, which means that the embedding is faithful to the diffusion flow in the tissues as the points are aligned along the diffusive pathways.

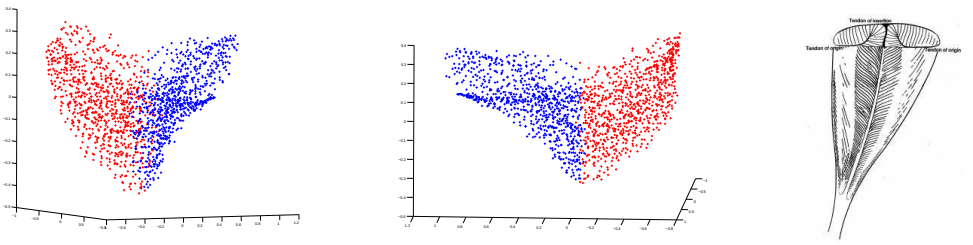

(a) (b) (c)

Figure 4: (a), (b) Two views of a three-dimensional embedding of the tensors of the soleus muscle, k-means clustering shows its bipennate structure. (c) Anatomy of the soleus [34].

5.1.2 Classification of the Muscle Groups

For each subject, a region of interest (ROI) was manually delineated and we tested the performance of the tensor clustering algorithm both for healthy and diseased subjects. In regions affected by myopathies, the tensors have a relatively small volume since fat replaces the fibers (as can be seen in [Fig.2 (b)]) and were eliminated through simple thresholding over the determinant. In all the experiments, we set the diffusion time t to $t = 2\ 10^5$ and we used a ten-dimensional embedding. For a quantitative evaluation of the method, we follow the validation protocol proposed in [9]: for all the 25 subjects, the manually delineated ROI was segmented at two different levels (in 7 and 10 classes). The resulting clusters are then classified according to the labels given by the expert. As in [9], several clusters are allowed to have the same label. We also test the algorithm on a section near the knee which is characterized by a higher amount of noise and artifact obtained automatically by a threshold (set to 20) on the diffusion-free images. We report in [Fig.6] the boxplots of the dice volume overlap with the expert labels for the 25 patients and its counterpart for the spectral clustering as described in the previous subsection. We can see that our algorithm performs slightly better for the case of the manually-delineated ROI, however for the noisy automatic ROI, spectral clustering is misled by isolated points (see [Fig.5 (c)]), whereas the performance of our algorithm is not significantly worsened. Note also that the thresholding over the determinant removes some of the tensors originating from the artifact. From a qualitative point of view, one can see in [Fig.5 (a), (b)] that the algorithm was able to segment correctly fine structures like AT and PL and the segmentation result is rather smooth.

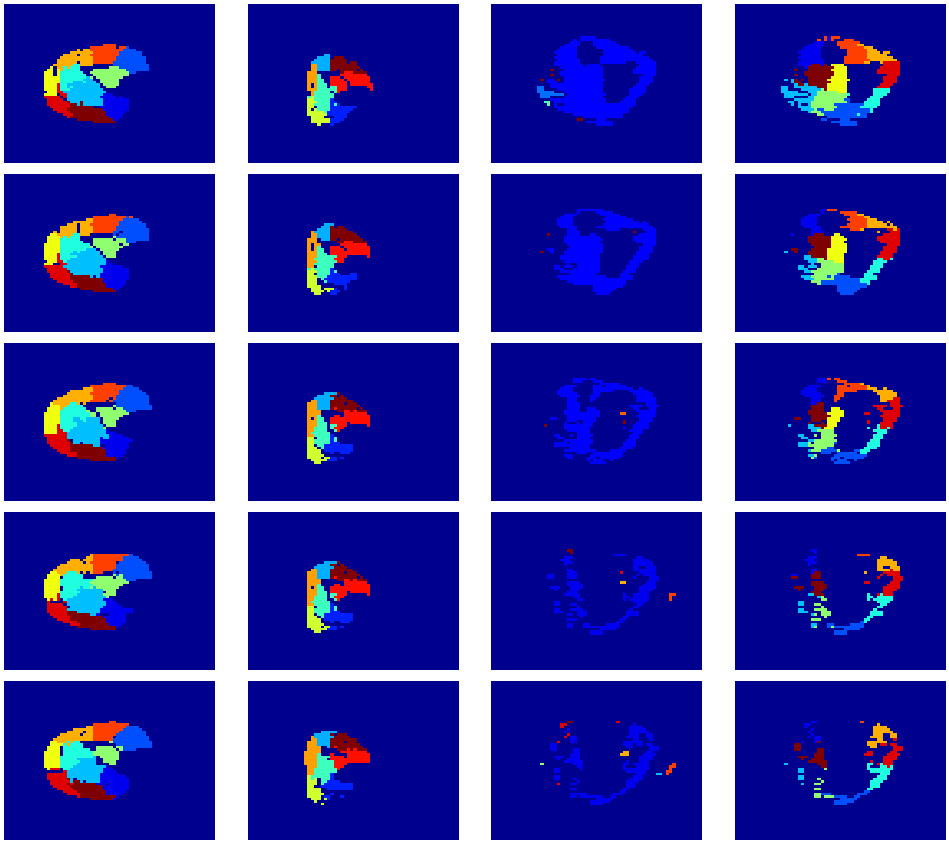

(a) (b) (c) (d)

Figure 5: Axial slices of the segmentation of the tensors for (a) a healthy subject in 10 classes, manual ROI (b) a diseased subject in 7 classes where the MG is partially affected, manual ROI (c) noisy automatic ROI of a section near the knee using spectral clustering (d) noisy automatic ROI using our method

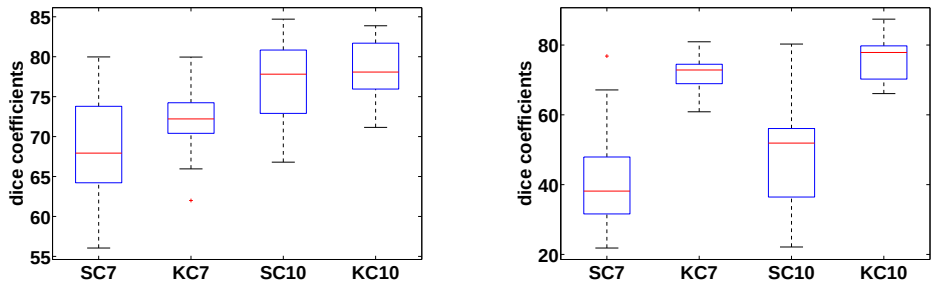

(a) (b)

Figure 6: Boxplot of the dice overlap coefficients for the 25 subjects for tensor clustering in 7 and 10 classes for (a) manual ROI and (b) automatic noisy ROI. SC7 (resp. SC10) refers to spectral clustering in 7 (resp. 10) classes and KC7 (resp. KC10) refers to kernel clustering in 7 (resp. 10) classes.

5.2 Fiber Clustering

5.2.1 Unsupervised Fiber Clustering

To test the unsupervised kernel-PCA clustering algorithm, we only kept the fibers which have a majority of points lying in the manually delineated ROI. The number of fibers in the different datasets ranged approximately from 1000 to 2500, which makes the computation and eigenanalysis of the kernel matrix achievable in a rather reasonable time. The diffusion time t was set to $t = 2\ 10^4$ and we used a ten-dimensional embedding for kernel-PCA. Figure 7 shows the clustering results in 10 (resp. 7) classes for the fiber tracts of a healthy (resp. diseased) subject. The fibers in [Fig.7 (a)] correspond to the tensors segmented in [Fig.5 (a)]. It is interesting to notice that despite the fact that the tractography algorithm was unable to recover fiber tracts in the diseased regions due to the presence of degenerate tensors, the clustering algorithm could still segment the fiber tracts of the healthy region in anatomically relevant subgroups. For quantitative assessment, we report in [Fig.8 (a)] the boxplot of the dice overlap measures of the fiber segmentation with the expert labeling for the 25 subjects for 7 and 10 classes. Overall, the algorithm performs well in separating the regions of the calf muscle with a mean dice coefficient of 79.5% (respectively 80.93%) and a standard deviation of 5.04% (respectively 5.14%) for 7 (respectively 10) classes.

5.2.2 Supervised Fiber Clustering

A manually segmented volume was used as an atlas. Atlas fibers were assigned to a class based on a simple voting procedure: each fiber is classified according to the majority vote class of the voxels it crosses. We experimented both with affine [33] and deformable [35]

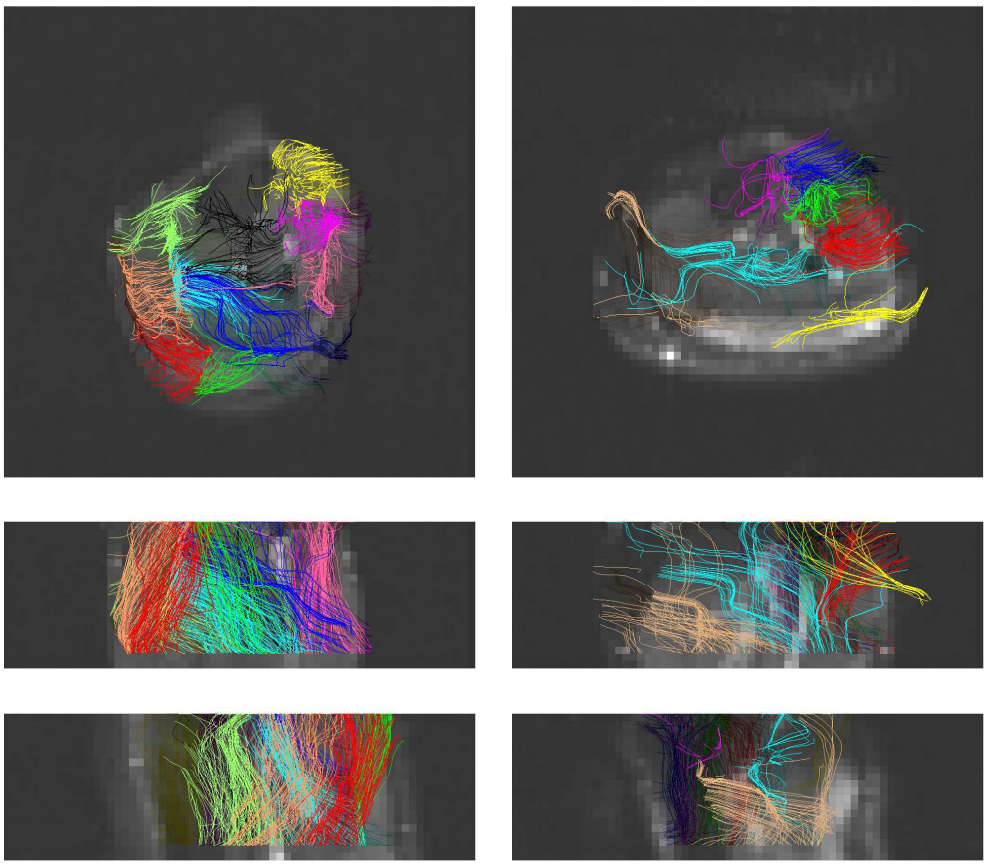

(a) (b)

Figure 7: Axial, coronal and saggital views of fiber segmentation for (a) a healthy subject in 10 classes, (b) a diseased subject in 7 classes.

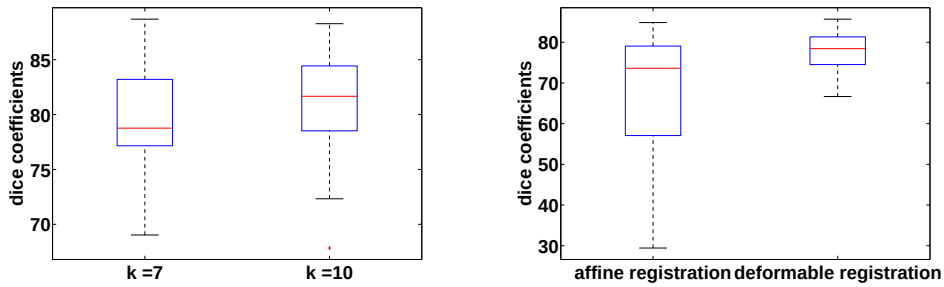

Figure 8: Boxplot of the dice overlap coefficients for the 25 subjects for (a) unsupervised fiber clustering in 7 and 10 classes, (b) supervised fiber clustering using affine and deformable registration.

registration to map the B0 images of the testing case to the B0 images of the atlas. We use kernel SVM classification to learn the fibers of the atlas as explained in section 4.2, using 21 one-against-one pairwise classifiers. The scale parameter in the Gaussian correlation kernel was set to $\sigma = 2\sqrt{\mu t} = 10$. We report in [Fig.8 (b)] the boxplot of the dice overlap coefficients both for deformable and affine registration. We can note that we obtain significantly better results with deformable registration, which was expected given the relatively high inter-patient variability and that muscles are soft tissues, so the anatomy and shape are likely to vary significantly across patients. In [Fig.9 (a)], we show an example of supervised segmentation compared with the ground truth in [Fig.9 (b)]. We can observe that as opposed to the unsupervised setting ([Fig.7 (a)]), the MG is not oversegmented.

6 Conclusion

In this report, we proposed a kernel-based method for clustering of both tensors and fibers in diffusion tensor images. It exploits the physical interpretation behind the modality and offers a unified approach towards tensor and fiber grouping. The kernel defined over the tensor space encompasses both localization and diffusion information and naturally reflects tensor alignment along fiber tracts. We showed its flexibility by extending it to deal with fibers and gave the physical intuition behind its mathematical definition as a kernel over sets of tensors. We also showed how to include expert knowledge by means of kernel SVMs.

Future research will focus on the use of the defined kernels for (affine or deformable) registration of diffusion tensors and will explore the possible extensions of the fiber kernel using stochastic process theory, in particular Gaussian processes. The motivation of the work is to use diffusion tensor imaging in order to detect and monitor the progression of skeletal muscle diseases like myopathies.

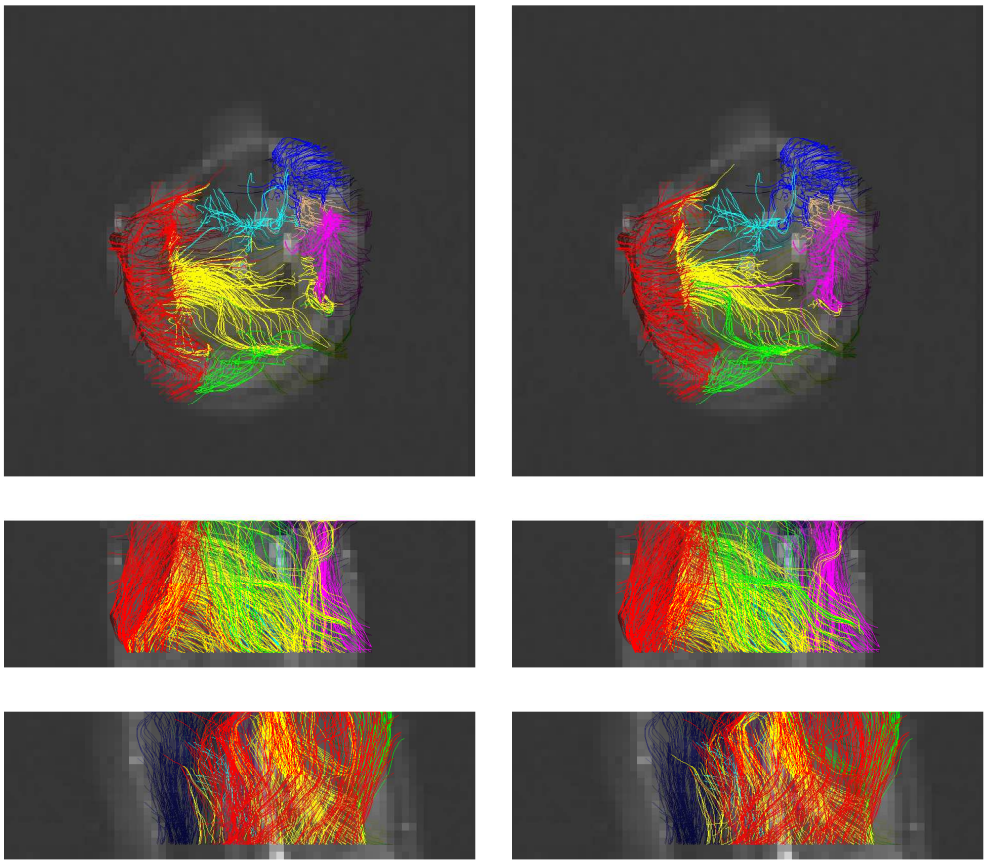

(a) (b)

Figure 9: Axial, coronal and saggital views for (a) supervised classification in 7 classes (b) the ground truth segmentation.

References

[1] Denis Le Bihan, Jean-Francois Mangin, Cyril Poupon, Chris A. Clark, Sabina Pappata, Nicolas Molko, and Hughes Chabrait, "Diffusion tensor imaging: Concepts and applications", *Journal of Magnetic Resonance Imaging*, vol. 13, pp. 534–546, 2001.

[2] C. Lenglet, M. Rousson, and R. Deriche, "DTI segmentation by statistical surface evolution", *IEEE TMI*, vol. 25, no. 06, pp. 685–700, 2006.

[3] Zhizhou Wang and Baba C. Vemuri, "DTI segmentation using an information theoretic tensor dissimilarity measure", *IEEE TMI*, vol. 24, no. 10, pp. 1267–1277, 2005.

[4] John Melonakos, Vandana Mohan, Marc Niethammer, Kate Smith, Marek Kubicki, and Allen Tannenbaum, "Finsler tractography for white matter connectivity analysis of the cingulum bundle", in *MICCAI*, 2007.

[5] L. Jonasson, P. Hagmann, C. Pollo, X. Bresson, C. Richero Wilson, R. Meuli, and J. Thiran, "A level set method for segmentation of the thalamus and its nuclei in DT-MRI.", *Signal Processing*, vol. 87, no. 2, pp. 309–321, 2007.

[6] Suyash P. Awate, Hui Zhang, and James C. Gee, "A fuzzy, nonparametric segmentation framework for DTI and MRI analysis: With applications to DTI-tract extraction", *IEEE TMI*, vol. 26, no. 11, pp. 1525–1536, 2007.

[7] Ye Duan, Xiaoling Li, and Yongjian Xi, "Thalamus segmentation from diffusion tensor magnetic resonance imaging", *Journal of Biomedical Imaging*, vol. 2007, no. 2, pp. 1–1, 2007.

[8] Yonas T. Weldeselassie and Ghassan Hamarneh, "DT-MRI segmentation using graph cuts", 2007, SPIE Medical Imaging.

[9] Ulas Ziyan, David Tuch, and Carl-Fredrik Westin, "Segmentation of thalamic nuclei from DTI using spectral clustering", in *MICCAI*, 2006.

[10] Alvina Goh and Rene Vidal, "Clustering and dimensionality reduction on Riemannian manifolds", in *CVPR*, 2008.

[11] Alvina Goh and Rene Vidal, "Segmenting fiber bundles in diffusion tensor images", in *ECCV*, 2008.

[12] A. Brun, H. Knutsson, H. J. Park, M. E. Shenton, and C.-F. Westin, "Clustering fiber tracts using normalized cuts", in *MICCAI*, 2004.

[13] Lauren ODonnell and Carl-Fredrik Westin, "White matter tract clustering and correspondence in populations", in *MICCAI*, 2005.

[14] Anders Brun, Hae-Jeong Park, Hans Knutsson, and Carl-Fredrik Westin, "Coloring of DT-MRI fiber traces using Laplacian eigenmaps", in *EUROCAST*, 2003.

[15] Andy Tsai, Carl-Fredrik Westin, Alfred O. Hero, and Alan S. Willsky, "Fiber tract clustering on manifolds with dual rooted-graphs", in *CVPR*, 2007.

[16] M. Maddah, W. Grimson, S. Warfield, and W. Wells, "A unified framework for clustering and quantitative analysis of white matter fiber tracts", *Medical Image Analysis*, vol. 12, no. 2, pp. 191–202, 2008.

[17] Peter Savadjiev, Jennifer S. W. Campbell, G. Bruce Pike, and Kaleem Siddiqi, "Streamline flows for white matter fibre pathway segmentation in diffusion MRI", in *MICCAI*, 2008.

[18] Mahnaz Maddah, Andrea U. J. Mewes, Steven Haker, W. Eric L. Grimson, and Simon K. Warfield, "Automated atlas-based clustering of white matter fiber tracts from DTMRI", in *MICCAI*, 2005.

[19] Lauren ODonnell and Carl-Fredrik Westin, "Automatic tractography segmentation using a high-dimensional white matter atlas", *IEEE TMI*, vol. 26, no. 11, pp. 1562–1575, 2007.

[20] Tony Jebara, Risi Kondor, and Andrew Howard, "Probability product kernels", *Journal of Machine Learning Research*, vol. 5, pp. 819–844, 2004.

[21] Xavier Pennec, Pierre Fillard, and Nicholas Ayache, "A Riemannian framework for tensor computing", *International Journal of Computer Vision*, vol. 66, no. 1, pp. 41–66, 2006.

[22] Bernhard Scholkopf, Alexander Smola, and Klaus-Robert Muller, "Nonlinear component analysis as a kernel eigenvalue problem", *Neural Comp.*, vol. 10, no. 5, pp. 1299–1319, 1998.

[23] J. B. Tenenbaum, V. de Silva, and J. C. Langford, "A global geometric framework for nonlinear dimensionality reduction.", *Science*, vol. 290, no. 5500, pp. 2319–2323, 2000.

[24] Vin de Silva and Joshua B. Tenenbaum, "Global versus local methods in nonlinear dimensionality reduction", in *NIPS*, 2002, pp. 705–712.

[25] David Haussler, "Convolution kernels on discrete structures", Tech. Rep., 1999.

[26] Yanghai Tsin, *Kernel Correlation as an Affinity Measure in Point-Sampled Vision Problems*, PhD thesis, Robotics Institute, Carnegie Mellon University, 2003.

[27] V. Vapnik, *Statistical Learning Theory*, Wiley, 1998.

[28] Nikos Komodakis, Georgios Tziritas, and Nikos Paragios, "Fast, approximately optimal solutions for single and dynamic MRFs.", in *CVPR*, 2007.

[29] Craig J. Galban, Stefan Maderwald, Kai Uffmann, Armin de Greiff, and Mark E. Ladd, "Diffusive sensitivity to muscle architecture: a magnetic resonance diffusion tensor imaging study of the human calf", *European Journal of Applied Physiology*, vol. 93, no. 3, pp. 253 – 262, 2004.

[30] Usha Sinha and Lawrence Yao, "In vivo diffusion tensor imaging of human calf muscle", *Journal of Magnetic Resonance Imaging*, vol. 15, no. 1, pp. 87–95, 2002.

[31] Damon BM, Ding Z, Anderson AW, Freyer AS, and Gore JC, "Validation of diffusion tensor mri-based muscle fiber tracking", *Magnetic Resonance in Medicine*, vol. 48, pp. 97–104, 2002.

[32] Radhouene Neji, Gilles Fleury, Jean Francois Deux, Alain Rahmouni, Guillaume Bassez, Alexandre Vignaud, and Nikos Paragios, "Support vector driven Markov random fields towards DTI segmentation of the human skeletal muscle.", in *ISBI*, 2008.

[33] Pierre Fillard, Nicolas Toussaint, and Xavier Pennec, "Medinria: DT-MRI processing and visualization software", Similar Tensor Workshop, 2006.

[34] Nick Milne, "Human functional anatomy 213", `http://www.lab.anhb.uwa.edu.au/hfa213/week3/lec3unimuscle.pdf`.

[35] B. Glocker, N. Komodakis, G. Tziritas, N. Navab, and N. Paragios, "Dense image registration through mrfs and efficient linear programming", *Medical Image Analysis*, vol. 12, no. 6, pp. 731–741, 2008.

Unité de recherche INRIA Futurs
Parc Club Orsay Université - ZAC des Vignes
4, rue Jacques Monod - 91893 ORSAY Cedex (France)

Unité de recherche INRIA Lorraine : LORIA, Technopôle de Nancy-Brabois - Campus scientifique
615, rue du Jardin Botanique - BP 101 - 54602 Villers-lès-Nancy Cedex (France)
Unité de recherche INRIA Rennes : IRISA, Campus universitaire de Beaulieu - 35042 Rennes Cedex (France)
Unité de recherche INRIA Rhône-Alpes : 655, avenue de l'Europe - 38334 Montbonnot Saint-Ismier (France)
Unité de recherche INRIA Rocquencourt : Domaine de Voluceau - Rocquencourt - BP 105 - 78153 Le Chesnay Cedex (France)
Unité de recherche INRIA Sophia Antipolis : 2004, route des Lucioles - BP 93 - 06902 Sophia Antipolis Cedex (France)

Éditeur
INRIA - Domaine de Voluceau - Rocquencourt, BP 105 - 78153 Le Chesnay Cedex (France)

ISSN 0249-6399